Chapter I

I.1 Introduction

Energy consumption is an important parameter that indicates the development and economic status of a society. According to the latest report of natural resources defence council (NRDC) [1], more than 60% of the electricity is generated using non-renewable sources such as oil, gas, and coal **(Figure I.1(a))**. Unearthing, processing, and moving underground oil, gas, and coal deposits take an enormous toll on our ecosystem. Burning of fossil fuels to fulfil energy demand adversely affects the environment by releasing greenhouse gases in earth's atmosphere, increasing the global average temperature. At the same time, the reserves of fossil fuels are also depleting. To reduce the burning of fossil fuels, alternative renewable energy sources, such as wind energy, tidal energy, geothermal energy, hydro-energy, biomass energy, and solar energy, are being explored. Out of all the renewable energy resources, solar energy is the most abundant source of energy that can be harvested with the minimum requirement of maintenance.

The total consumption of energy by the world was ~15.70×10^{13} kWh in the year 2020 (Enerdata, 2020) **(Figure I.1(b))**. EIA projects a nearly 50% increase in world energy use by 2050 (Source: U.S. Energy Information Administration (EIA), International Energy Outlook 2021). According to EIA, solar energy will play a pivotal role in fulfilling the future electricity demand. If the uninhabited areas are ignored, the amount of solar energy received by land is about 163.16×10^{12}

kWh/day. Even if this energy is harvested at a meagre 5% efficiency, $300x10^{13}$ kWh/year can be generated, which is 20 times more than estimated world energy demand for the year 2020 ($15.70x10^{13}$ kWh/year). The key to the large-scale implementation of solar photovoltaics is the cost of electricity which is already below the grid electricity cost per unit. With the improving performance of solar cells, the per-unit electricity cost is expected to reduce further.

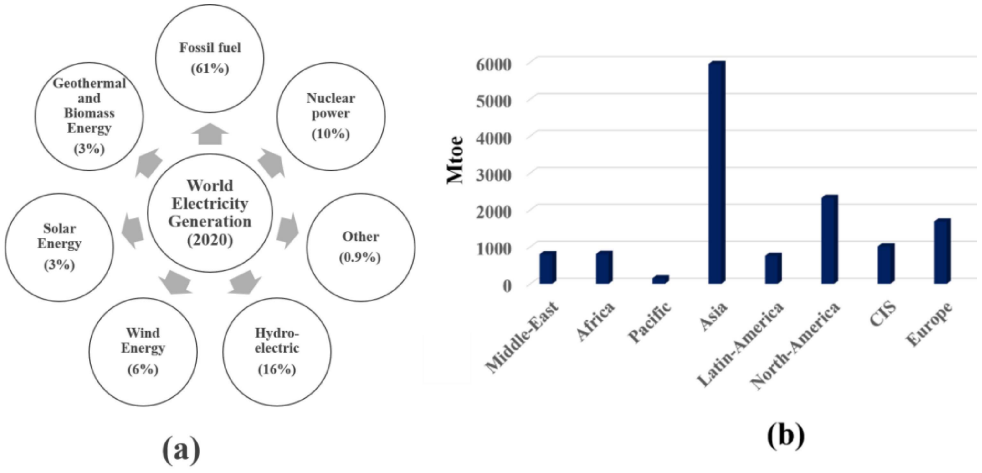

Figure I.1 (a) Percentage of total electricity produced by the world using renewable and non-renewable sources, (b) Total energy consumption over the world in the year 2020 (Mtoe: megatonne of oil equivalent). Data adapted from Ref. [1] and [2].

I.2 Evolution of Solar Cell Technology

Solar cells work on the principle of the photovoltaic effect, discovered by Edmond Becquerel in the year 1839 [3]. It was found that when the light was shown upon the electrode (silver) dipped in an acidic medium, the current flows through the electrode; this is known as Becquerel effect. Later in 1877, Adams and Day [4] observed a reduction in resistance of a selenium bar when exposed to light. In 1883,

Fritts *et al.* [5] demonstrated the first thin film selenium solar cell by pressing a thin selenium sheet (25μm) in between a gold and a brass plate and allowing light to fall on the selenium plate. A current was observed to flow through the external circuit when Se sheet was exposed to light. Ohl *et al.* [6] made the first patent for silicon solar cells in 1941 with an efficiency of less than 1%. Later, Chapin *et al.* [7] achieved 6% efficiency in a silicon solar cell. Since then, several different solar cell technologies have evolved with Si, GaAs, CIGS and, more recently, perovskite absorber based solar cells demonstrating close to 25% efficiency.

I.3 Principle of Solar Cell Operation

A solar cell is a device used to convert solar energy into electrical energy by utilizing photovoltaic effect. In simple terms, a solar cell is a p-n junction formed by coupling a p-type semiconductor and an n-type semiconductor **(Figure I.2(a))**. All semiconductors have a bandgap in their electronic structure and can thus excite an electron from the valance band to conduction band. Yet, only a select group has bandgap suitable to absorb solar light. A solar cell absorb photons (light) having energy greater than the bandgap ($E>E_g$) of the absorber layer and generates electron-hole pairs. The generated charge carriers are separated by a built-in electric field across the junction and are collected at the electrodes. For the standard AM 1.5G solar spectrum, the ideal bandgap (E_g) of absorber materials is between 1-1.5 eV.

A device with a single p-n junction is called a diode. When an n and p-type semiconductor is brought in contact to form a p-n junction, the in-built concentration gradient pushes the electrons from the n-type to the p-type while the

hole is pushed in the opposite direction. The flux of the charge carriers under the influence of concentration gradient is called diffusion current (I_{diff}). The region close to junction depleted of majority charge carriers due to diffusion is called depletion region or space charge region **(Figure I.2(b))**. The movable charge carriers no longer balance the ionized impurities in the depletion region. This builds up a net positive charge on the n-side and a net negative charge on the p-side of the junction. The charge built up causes a potential difference across the junction resulting in an internal electric field **(Figure I.2(c))** from the n to the p region. The electric field opposes the drift current. The flux of charge carriers because of the electric field is known as drift current (I_{drift}). The magnitude of the electric field is given by

$$\varepsilon = \frac{-dV(x)}{dx} \qquad \textbf{I.1}$$

where, V is the potential across the junction. The potential difference across n and p-type semiconductors called the built-in potential barrier **(Figure I.2(d))** which is given by:

$$V_{bi} = \frac{KT}{q} \ln \left(\frac{N_d N_a}{n_i^2} \right) \qquad \textbf{I.2}$$

where, V_{bi}, N_a, N_d, n, KT/q, T and q are built-in potential in volts, acceptor impurity, donor impurity concentration, concentration of electron, thermal voltage, temperature in kelvin and charges in Coulombs respectively. The built-in potential barrier for silicon solar cell is about 0.7 eV, which means > 0.7 eV energy is required for the electron in the conduction band to move across the junction. The p-n junction is said to be in equilibrium when chemical potential which is measured

as Fermi level, E_f, is at same energy throughout the junction. This results in the bending of the energy band across the junction, as shown in **Figure I.2(e)**.

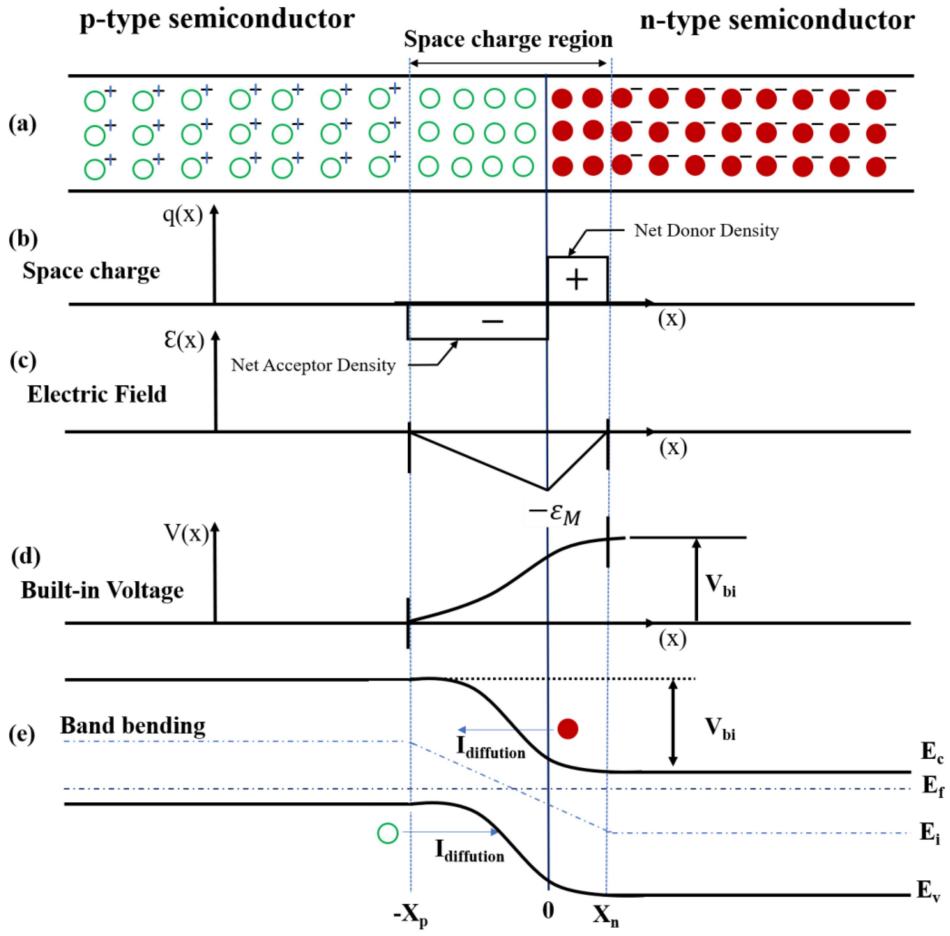

Figure I.2 (a) p-n junction formation, (b) Space charge distribution of a p-n junction in equilibrium, (c) Electric field and (d) Potential distribution of an abrupt p-n junction, (e) Energy band diagram of a p-n junction in the thermal equilibrium.

If a relatively positive voltage is applied to the p-type semiconductor of the p-n junction, the junction barrier potential is reduced. This configuration is known as the forwards biased. On applying a forward biased, the built-in electric potential in the depletion region is reduced and I_{diff} of majority carriers increases, while no

significant change in I_{drift} happens due to the limited number of minority charge carriers. On the other hand, when a positive voltage is applied to the n-type semiconductor (known as the reverse bias) built-in electric potential across the space charge region increases and opposes the diffusion of majority carriers. Therefore, I_{diff} decreases dramatically; however, a small increase in the I_{drift} is experienced due to the small increase in the width of the space charge region but is still limited by the generation of minority carriers. The current density-applied voltage (J-V) characteristics is known as the diode behaviour, and it is represented by the following equation I.3 [8, 9]:

$$J = J_o \left[exp\left(\frac{qV}{nkT}\right) - 1 \right] \qquad \textbf{I.3}$$

where, J_o, q, V, n, k, and T are dark saturation current or diode leakage current in the absence of light, electronic charge, the applied voltage across the terminals of the diode, ideality factor, Boltzmann's constant and temperature, respectively. When a p-n junction is illuminated, the p-n junction operates in superposition [10]. An equivalent circuit diagram for the ideal solar cell is shown in **Figure I.3(a)**, where a current source is connected in parallel with a rectifying diode. The J-V characteristics curve can be obtained from the corresponding characteristic of a diode in the dark, as shown in **Figure I.3(b)**. Under illumination, charge pairs are generated, which increases the minority carrier density in the depletion region, resulting in increased drift current and shifting the characteristic curve along the current density axis as shown in **Figure I.3(b)**. The total current density for the solar cell is the summation of the photogenerated current and the dark current as described by the equation I.4:

$$J = J_o \left[exp\left(\frac{qV}{nkT}\right) - 1 \right] - J_L \qquad \textbf{I.4}$$

Photo generated current density (J_L) can be equated with the current flowing through the shorted outer circuit (J_{sc}). The short circuit current is generally expressed per unit active cell area and is known as short circuit current density (J_{sc}). When a solar cell is illuminated while the outer circuit is open, the generated free charge carriers flow through the built-in electric field of the device and charge built up on the other side of the junction. The charge built-up by photogenerated carriers continues to increase till it just balances the built-in field. At this stage, the built-in field will not be able to separate charge carriers anymore. The corresponding built-up potential across the device is called open-circuit voltage (V_{OC}), and it is the maximum voltage a cell can provide. V_{OC} is given by the equation I.5:

$$V_{oc} = \frac{KT}{q}\left[\ln\left(\frac{J_L}{J_o}\right) + 1\right] \approx \frac{KT}{q}\ln\frac{J_L}{J_o} \qquad \textbf{I.5}$$

In general, parameters which are used to evaluate the performance of solar cell include short circuit current (J_{SC}), open-circuit voltage (V_{OC}), fill factor (FF), power conversion efficiency (PCE, η), and quantum efficiency (QE). Other factors which directly influence the performance includes parasitic resistance, series resistance (R_S) and shunt resistance (R_{Sh}). In an ideal case, the solar cell short circuit current is equal to the photocurrent. The cell efficiency (η) is computed from the maximum power density delivered by the cell ($J_{mp}V_{mp}$) relative to the irradiated power density $P_{in,}$ as per the equation I.6:

$$\eta = \frac{P_{max}}{P_{in}} = \frac{I_{mp}V_{mp}}{P_{in}} = \frac{J_{sc}V_{vo}FF}{P_{in}} \qquad \textbf{I.6}$$

where the fill factor FF, which is defined as:

$$FF = \frac{I_{mp}V_{mp}}{J_{sc}V_{vo}} \qquad \textbf{I.7}$$

The FF describes how closely the area defined by the *J–V* curve resembles a rectangle **(Figure I.3(b))**. The obvious reasons for poor FF can be large R_S, small R_{Sh}, and voltage-dependent carrier collection.

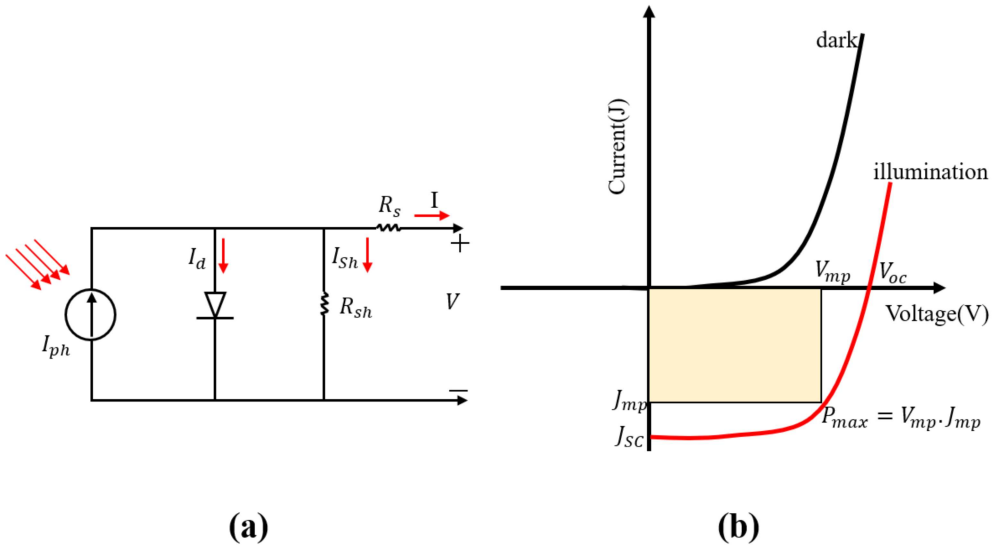

Figure I.3 (a) Equivalent circuit diagram of a photovoltaic cell: a current source in parallel with a diode, (In practice, no solar cell is ideal so a shunt resistance (R_{Sh}) and a series resistance (R_S) are also included), (b) *J-V* characteristics under dark and light conditions.

The quantum efficiency (QE) represents the ratio of number of electrons collected by solar cell to incident photon at each wavelength. QE remains zero for photons

with energy below bandgap (E_g) of the absorber material. The external quantum efficiency (EQE) includes the effect of both the electronic losses during photogeneration and collection in absorber, while optical losses refer to the absorption and reflection in window, transparent conductor, and other layers. Since the optical losses do not change with applied bias, comparing external quantum efficiencies at different bias voltages is meaningful to separate electronic losses and optical losses, providing insight into the recombination mechanism in the solar cells. Ideally, photocurrent can be calculated by integrating EQE with respect to the wavelength.

I.4 Solar Cell: Absorber Material

Solar cells can be classified into wafer-based and thin-film technologies. The wafer-based solar cells are made from slices of semiconducting wafers derived from ingots. Crystalline silicon, GaAs, GaInP absorber materials are examples of wafer-based solar cell. The thin-film solar cell has a different approach in which cheaper and insulating substrates are used to deposit thin layers (usually a micron thin) of p and n-type material. CIGS, CZTS, a-Si:H, CdTe, etc. absorber based solar cells are examples of thin-film solar cells.

I.4.1 Wafer-based Solar Cell

In most wafer-based solar cells, silicon (Si) is the absorber material of choice. The wafers are produced by slicing high purity silicon ingots using wire saws. Silicon has close to the ideal bandgap (1.12 eV) for sunlight absorption. Despite the indirect nature of its band gap, the silicon solar cells have achieved a high photoconversion efficiency mainly due to the material quality and technical knowledge base

borrowed from the already mature semiconductor industry. Crystalline-Si (c-Si) solar cells have several advantages, such as abundant raw material supply, low toxicity, low cost, and scalable technologies for cell and module fabrication. Crystalline silicon absorber can be either polycrystalline or monocrystalline. Schematic of a silicon-based solar cell architecture is shown in **Figure I.4(a)**. Single crystalline Si modules are among the most efficient, with the record lab-scale efficiency as high as 27.6 [11] and 26.1% [12] with and without concentrators, respectively. However, they are expensive as they require the highest purity silicon and involve complicated manufacturing processes [13].

On the other hand, the polycrystalline silicon (poly-Si) cells are cheaper to produce; however, they are comparatively less efficient than the single-crystalline Si solar cell. Silicon-based heterojunction solar cells (Si-HIT) were initially developed by Sanyo (now Panasonic), Japan in the year 2000 by using an amorphous Si (a-Si) layer to passivate the c-Si surface. The highest reported Si-HIT cell efficiency is 26.7% by K. Yoshikawa and his group [14]. Wafer-based silicon solar cells are called first-generation solar cells. Si-based solar cells have some drawbacks. As an indirect bandgap semiconductor, Si is a poor absorber of light and requires a fairly thick layer (~375 microns), making it bulky and rigid. Crystalline-Si includes the high-level requirements for material purification, the module form factor restrictions, batch-based cell production and module integration of processes with fairly low throughput. Current research areas are targeted at manufacturing wafer-based solar cells at lower costs and reduced complexity, increased modular conversion efficiencies, reduction in the quantity of silicon used per watt and the reliance on silver for contact metallization. Silicon-based solar cell accounts for

greater than 80% of the present market share **(Figure I.4(b))**; however, due to their rigidity, inefficient light absorption, and requirement of costly processing, other types of solar devices are also being explored.

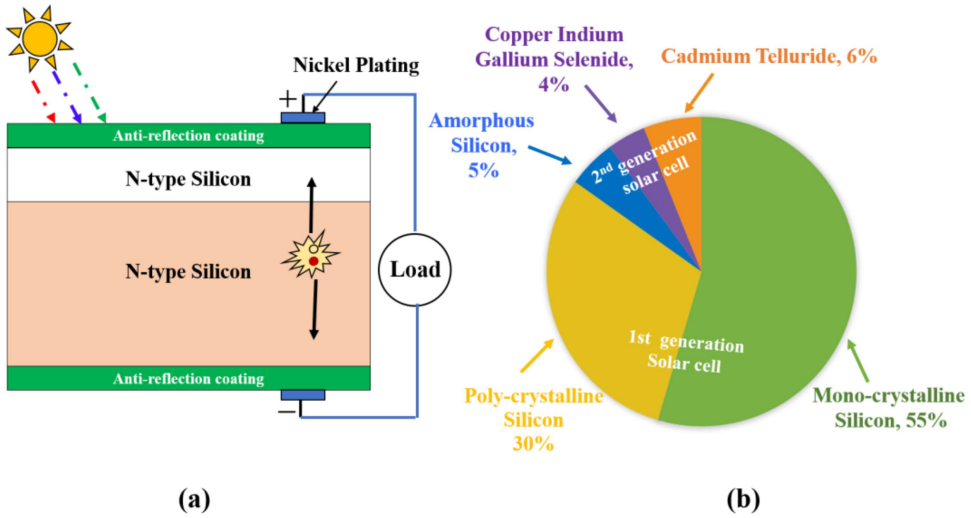

Figure I.4 (a) Schematic of silicon-based PVs device structure, (b) Market share of PVs panels by technology type. Data source: IEA, USA.

I.4.2 Thin-film Solar Cells

The journey of thin-film solar cells (TFSCs) started during 1970s. Ease in manufacturing, flexibility, and low cost are the main drivers of thin-film PV technologies. The most notable TFSC technologies include hydrogenated amorphous silicon (a-Si:H), cadmium telluride (CdTe), copper indium gallium diselenide ($CuInGaSe_2$), copper zinc tin sulfide (CZTS), dye-sensitized solar cells (DSSCs), organic photovoltaics (OPV), colloidal quantum dot photovoltaics (QDPV) and perovskite solar cell. TFSC can be processed at lower temperatures (typically less than 550 °C). Most of the thin film absorbers can be processed by

solution-based processing, which are scalable and cheaper. Out of all TFSCs technology, only three technologies: hydrogenated amorphous silicon (a-Si:H), cadmium telluride (CdTe), copper indium gallium diselenide ($CuInGaSe_2$) cells, have been commercialized. These thin-film solar cells are referred as second-generation solar cells and have nearly 15% of the market share, as depicted in **Figure I.4(b)**. The 2nd generation TFSCs are based on direct bandgap materials with a high absorption coefficient and, therefore, require a very thin layer (1-10 micron) of absorber material. Because of being thin, these cells can be flexible and are also less prone to damage than their c-Si rivals. Large area coatings are also possible at high throughput and low costs and can be deposited on cheaper substrates such as sola-lime glass (SLG), steels, and polymer substrates. A variety of processing techniques have been applied for depositing thin-film absorber layer, which include thermal evaporation, sputtering, chemical vapour deposition, spray deposition. The highest reported PCE for a-Si, CdTe and CIGS are 13.6, 22.1 and 23.4%, respectively.

I.4.3 Copper Indium Gallium Diselenide

Among all commercial thin-film technologies, $CuIn_xGa_{1-x}(Se)_2$ stands out as the fastest growing with the highest power conversion efficiency, as shown in **Figure I.5(a)**. CIGS absorber layer has direct and tunable bandgap (1.04 eV for $CuInSe_2$ to 2.0 eV for $CuGaSe_2$) [15, 16], high optical absorption coefficients in the visible light region ($\approx 10^5$ cm^{-1}) [17] **(Figure I.5(b))** with absorption in the entire visible and near IR range **(Figure I.5(c))**. As a result, 1-2 μm thick absorber layers are sufficient to absorb all the incident light [18, 19]. A schematic of the commercial CIGS TFSC architecture is shown in **Figure I.5(d)**. CIGS has also been explored

for space application as a substitute cost-intensive GaAs cell due to its greater stability under high energy radiation. Efficiency as high as 24% has been reported for a single-junction CIGS cell [20].

The CIGS absorber layer can be synthesized by vacuum-based processing such as evaporation and sputtering or by solution-based technologies such as spray deposition, screen printing, and slot-die casting. In most cases, the high performance cells (>20%) have been fabricated using the CIGS absorber layers processed through vacuum-based processing methods (mainly co-evaporation and sputtering) [21–23]. The vacuum-based deposition process has the benefit of control over composition and high-quality absorber layers. However, it requires a high energy input, large capital investments, and operational costs at the same time are not easily implementable for industrial-scale processing [24, 25]. In addition, it is also challenging to maintain the stoichiometry of indium (In) and gallium (Ga). These drawbacks are inherent barriers to large-scale, high-throughput production of CIS/CIGS-based solar cells. Solution processing has been projected as a viable option for depositing CIGS absorber layer [15, 26–28]. CIGS absorber layers have been deposited by solution-based processes (spray coating, inkjet printing etc.). However, the highest efficiency achieved by any solution-based processing technique is much lower (~18.7% by Solar frontier) than that deposited by co-evaporation (24%).

Solution-based processing techniques can be classified based on the state of the ink i.e. molecular precursor ink (MI) and nanoparticle (NP) ink. In the case of the MI route, the metal chloride, acetylacetonate, or nitrate precursors are dissolved in a suitable solvent such as hydrazine, DMSO, or DMF to form ink which is then coated

on the substrate and decomposed to form the absorber layer. While, in the NP route, first colloidal CIGS nanoparticles are prepared by melt atomization, solvothermal route, or hot injection methods, which is then dispersed in suitable solvent such as toluene, ethylenediamine, hexanethiol, dodecanethiol, oleylamine (OLA), etc., to form colloidal ink. The colloidal ink is then deposited to form the absorber layer. The nanoparticle route has the benefits of well-defined structure, high phase purity and stoichiometry, offering a range of tunable optical and electrical properties compared to the molecular ink processing route. Solar cell fabricated using absorber layer processing using molecular ink route has resulted in PCEs in the range of 14–19% depending upon the solvent utilized, as listed in **Table I.1**.

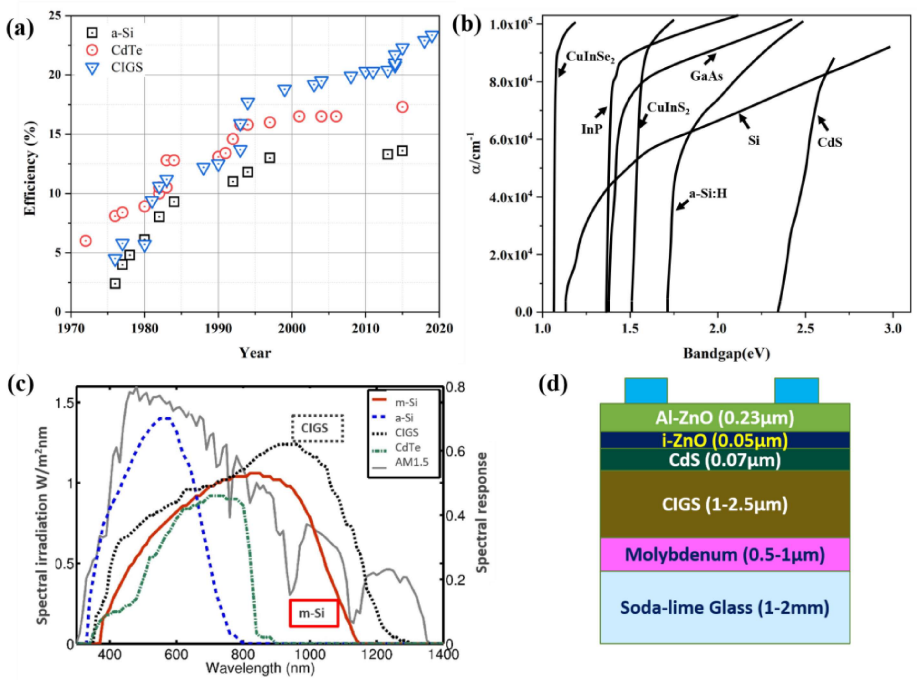

Figure I.5 (a) Progress in thin-film solar cell efficiencies of a-Si, CdTe and CIGS (Data adapted from Ref. [29] and [30]), (b) Absorption coefficient as a function of bandgap (Data adapted from Ref. [31]), (c) Spectral response of thin-film and

silicon solar cell over solar irradiance spectrum (Data adapted from Ref. [32]), (d) Schematic architecture of a CIGS solar cell.

Table I.1 List of the best PCEs achieved by fabricating solar cells utilizing the CIGS absorber layer processed through MI route.

Solvent utilized for processing CIGS absorber layer	**Highest reported PCE (%)**
Hydrazine[33]	18.1
DMF [34]	15.2
DMSO [35]	18.7
Methanol[36]	14.4
EDT[37]	16.4

On the other hand, the highest reported efficiency for a solar cell fabricated using the absorber layer processed through the NP route is 17.1%, where a low-cost printing method was used to deposit a slurry mixture containing selenide powders and metal oxide NPs on flexible foil. Both the processing routes (MI and NP) generally involve four steps: I) ink formulation, II) solution deposition by a non-vacuum process, III) intermediate drying (in the air or inert environments) to evaporate the solvent and eliminate residual impurities, and IV) finally, selenization/sulfurization (500–600 °C) in an inert atmosphere to achieve a rapid grain growth and improve crystalline absorber layers, which intern improve the efficiencies.

I.5 Motivation

In the case of the NP route, the colloidal suspension contains highly reactive NPs that act as the driving force for the layer densification on phase transformation that can contribute to the significant increase in the PCEs. Recently, NPs based ink approach received attention in the Cu_2ZnSnS_4 (CZTS) system, where the deposition of CZTS is carried out through NPs ink-based route [38–43]. The NP suspension was made by dispersing synthesized metastable wurtzite (wz) CZTS NPs, which on annealing in selenium atmosphere, phase transformed to kesterite CZTSSe. Interestingly, this process resulted in fully sintered, compact and uniform CZTS thin films with large grains. CIGS has a similar structure as CZTS. The only difference is tin and zinc are arranged orderly in kesterite-CZTS; whereas, in CIGS, indium and gallium are randomly distributed, forming a chalcopyrite structure. Similar to CZTS, the wurtzite is a high-temperature phase for CIGS **(Figure I.6)** which is stable between 1045-1090 °C [44–46]. Wurtzite CIGS can be converted to the stable ch-CIGS by annealing at intermediate temperatures [47]. Due to the structural similarities with CZTS, CIGS is also expected to undergo phase transformation assisted grain growth on the selenization of wz-CIGS. In this respect, this thesis attempts to synthesized phase pure wz-$CuIn_xGa_{1-x}S_2$ NPs and explore the phase transformation assisted grain growth in wet-chemically processed CIGS films.

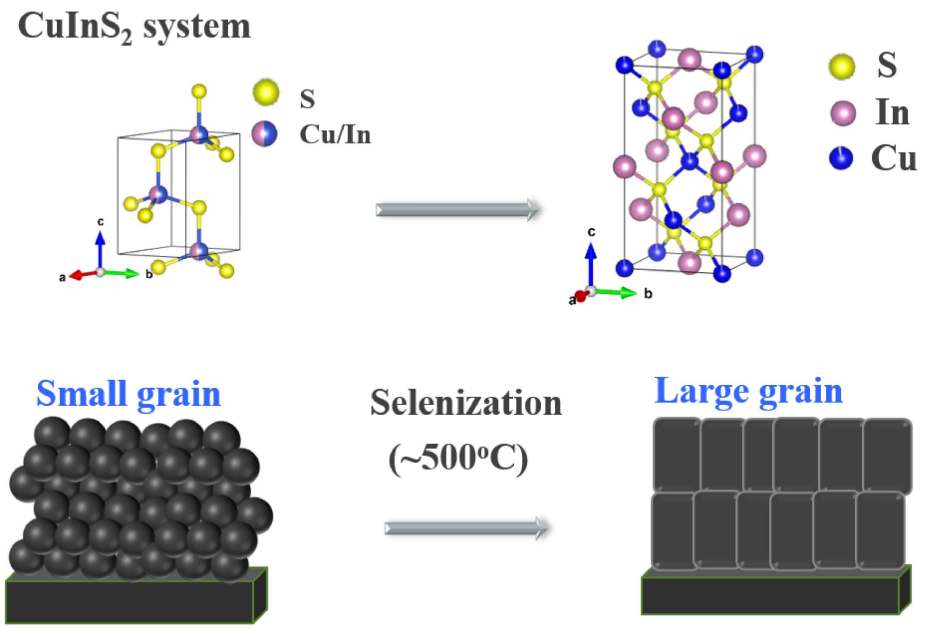

Figure I.6 Schematic of phase transformation assisted grain growth during selenization of wurtzite $CuInS_2$ absorber layer.

I.6 Challenges and Issues

There is a gap between lab-scale efficiency 23.35% and commercial module efficiency (18.6%). This difference is caused by inhomogeneity in the CIGS film over a large area. However, these best performances were reported by vacuum (co-evaporation and sputtering) mainly due to precise control over the composition during processing. Achieving similar homogeneity and precise control over chemical composition is challenging in solution-based processing. The synthesis of wz-CIGS nanoparticle and deposition conditions for nanoparticle ink must be carefully studied to yield a homogeneous chemistry, large grain morphology. The selenium partial pressure, temperature, and heating ramp rate are crucial for

achieving wurtzite to chalcopyrite phase transformation and grain growth to produce high-performance $CuIn_xGa_{1-x}(S, Se)_2$ absorber layers. Furthermore, the selenium vapour pressure must be regulated to control the Se diffusion into the $CuIn_xGa_{1-x}S_2$ and the thickness of the $MoSe_X$ film at the Mo/ $CuIn_xGa_{1-x}(S, Se)_2$ interface. The formation of a thin layer of $MoSe_2$ is beneficial for the adhesion of the CIS layer; however, a thick layer will block the carrier transport towards back contact. The use of inks with controlled stoichiometry and an optimized heat treatment process can facilitate grain growth, reduce residual impurities, film porosity, and improve thin-film morphology.

I.7 Scope and Objectives

Following is the scope of the present work:

1. To establish and study the formation mechanism of CIS wurtzite NPs
2. To prepare a wz-CIS colloidal ink for spray coating on the Mo-coated SLG and SLG substrate.
3. To optimize the deposition and selenization processes of wz-CIS to form high-performance ch-CISSe absorber layer.

To this end, the primary objectives of work are:

1) To synthesize the phase pure wurtzite CIS NPs through the hot injection method and in-depth analysis of the formation of wurtzite NPs.
2) To study the effect of the gallium addition in place of indium in the structure and mophology of wz-$CuIn_xGa_{1-x}S_2$.
3) To study the effect of various process parameters on the phase transformation and grain growth during the selenization.

4) To fabricate the thin film solar cell based on wurtzite CIS and chalcopyrite CISSe absorber layers.

I.8 Organization of the Thesis

This thesis focuses on solution processing of wurtzite $CuIn_xGa_{1-x}S_2$ nanoparticle which can be used as starting materials for spray deposition and selenization to achieve large-grained chalcopyrite-CIGS for application as absorber film for solar cells. The thesis is divided into eight chapters.

Chapter I presents a brief overview of the importance, working principle and evolution of solar cell technology. The chapter briefly describes different types of thin-film solar cells, including CIGS based solar cells. In the later part of the chapter, the need and motivation of the current investigation, significant challenges and objectives of the dissertation are described.

Chapter II presents a detailed discussion of the evolution, structure, and properties of the CIGS based PV absorber layer. The chapter also briefly discusses the cell architecture and the importance of different layers. Finally, the chapter discusses the state of the art of $CuIn_xGa_{1-x}(S,Se)_2$ absorber film deposition methods, emphasizing solution processing approaches.

Chapter III introduces material, processing methods and characterization/ analytical techniques utilized during the dissertation work.

Chapter IV describes the formation mechanism of metastable wz-$CuInS_2$ nanoparticles during solution processing. The role of amine-thiol at different states of nucleation and growth of nanoparticles is discussed.

Chapter V explores the substitution of gallium for indium ($CuIn_xGa_{1-x}S_2$ (x = 1, 0.7, 0.5, 0.3, 0)), and its influence on the structure and morphology of particles. The morphological evolution and its dependence on the composition In/Ga ratio is discussed.

Chapter VI focuses on selenization of spray deposited wz-CIS absorber layer to gain insight the phase transformation and grain growth.

Chapter VII describes the spray coating and optimization of various processing parameter to obtained homogeneous and dense film. Further, fabricated and charactrize the solar cell based on wz-CIS and ch-CISSe absorber layer.

Chapter VIII presents the overall summary and conclusions. Along with the conclusions, future prospects in this area are also discussed.